Available online at www.sciencedirect.com
ScienceDirect
Flow Measurement and Instrumentation 18 (2007) 107–113
Flow Measurement and Instrumentation
www.elsevier.com/locate/flowmeasinst

Experimental measurements of velocity and pressure distributions on a large broad-crested weir

Carlos A. Gonzalez[a,b], Hubert Chanson[c,*]

[a] Cardno, 5 Gardner Cl., Milton QLD 4064, Australia
[b] Department of Civil Engineering, The University of Queensland, Brisbane QLD 4072, Australia
[c] Hydraulic Engineering and Applied Fluid Mechanics, Division of Civil Engineering, The University of Queensland, Brisbane QLD 4072, Australia

Abstract

Basic experiments were conducted in a near full-scale broad-crested weir. Detailed velocity and pressure measurements were performed for two configurations. The results showed the rapid flow distribution at the upstream end of the weir, while an overhanging crest design may affect the flow field. The study showed further that large vortical structures might be observed immediately upstream of the weir and impact adversely on the overflow.

Keywords: Broad-crested weir; Velocity distributions; Pressure distributions; Vortices

1. Introduction

A broad-crested weir is a flat-crested structure with a crest length large compared to the flow thickness (e.g. [8,12,4]) (Fig. 1). When the crest is "broad", the streamlines become parallel to the crest invert and the pressure distribution is hydrostatic. The discharge above the weir equals

$$\frac{Q}{B} = C_D * \sqrt{g * \left(\frac{2}{3} * H_1\right)^3} \quad (1)$$

where Q is the discharge, B is the channel breadth, g is the gravity acceleration, H_1 is the upstream total head above the crest (Fig. 1), and C_D is the dimensionless discharge coefficient [9,5]. C_D is unity for an ideal fluid flow above the broad-crest.

The hydraulic characteristics of broad-crested weirs were studied during the 19th and 20th centuries. Table 1 summarises pertinent studies. Belanger [3] analysed the overflow theoretically. Early experimental studies included the contributions of Bazin [2] and of Woodburn [21]. Tison [20] studied the overflow above a broad crest experimentally and analytically. Serre [18] analysed the free-surface profile above the weir theoretically. Mos [13] analysed the flow separation at the upstream corner of square-edged broad-crested weirs numerically and experimentally. Hall [7] and Isaacs [10] studied the effects of developing boundary layer on the weir overflow. Ramamurthy, Tim and Rao [14] systematically studied the discharge characteristics of round-edged and square-edged weirs.

It is the purpose of this note to document pressure and velocity redistributions on a horizontal broad-crested weir with rounded nose. New experiments were performed in a near-full-scale facility. The results provide new insights into the vertical profiles of pressure and velocity in the upstream half of the broad-crest, including the boundary layer development and salient flow patterns.

2. Experimental apparatus

New experiments were conducted at the University of Queensland in a 7 m long, 1 m wide test section. The waters were supplied from a large 1.5 m deep feeding basin with a surface area of 6.8 m × 4.8 m leading to a sidewall convergent with a 4.8:1 contraction ratio. Thus an excellent, smooth and waveless inflow was obtained. Four broad-crested

* Corresponding author.
E-mail address: h.chanson@uq.edu.au (H. Chanson).

0955-5986/$ - see front matter © 2007 Elsevier Ltd. All rights reserved.
doi:10.1016/j.flowmeasinst.2007.05.005

Notation

B	channel breadth (m)
C_D	dimensionless discharge coefficient
d	water depth (m)
d_c	critical flow depth (m)
d_{crest}	depth (m) on the weir crest
g	gravity acceleration (m/s^2)
H	total head (m)
H_1	upstream total head (m) measured above the crest
h	weir height (m) above upstream channel invert
k_s	equivalent sand roughness height (m)
L	crest length (m) measured in the flow direction
L_{crest}	crest length (m) measured in the flow direction
Q	water discharge (m^3/s)
P	pressure
q	discharge per unit width (m^2/s)
R	radius of curvature (m)
V	velocity (m/s)
V_c	critical flow velocity (m/s)
Ø	diameter (m)
δ_{99}	boundary layer thickness (m)
ν	kinematic viscosity of water
ρ	water density (kg/m^3)

Subscripts

crest	crest flow conditions
1	upstream channel flow conditions
2	downstream channel flow conditions

weir geometries were tested (Table 1), but most detailed measurements were performed for Geometries 3 and 4. The third and fourth geometries consisted of a 1 m wide, 0.62 m long and 0.99 m high broad-crest with an upstream rounded corner (0.057 m radius). In Geometry 3, the inflow conditions were characterised by an overhanging crest (corbel) inflow (Fig. 1). Additional flow visualisations were carried out in a small glass channel with a 0.25 m wide broad-crested weir made of perspex.

A pump controlled with an adjustable frequency AC motor drive delivered the flow rate, enabling an accurate discharge adjustment in a closed-circuit system. Clear-water flow depths were measured with a point gauge. Pressure and velocity measurements were performed with a Prandtl–Pitot tube (Ø = 3.3 mm). The Pitot tube was connected to an inclined manometer which gave both total head and piezometric head. The translation of the Pitot–Prandtl probe in the vertical direction was controlled by a fine adjustment travelling mechanism connected to a Mitutoyo™ digimatic scale unit (Ref. No. 572-503). The error on the vertical position of the probe was less than 0.025 mm. The accuracy on the longitudinal position was estimated as $\Delta x < +/-0.3$ cm. The accuracy on the transverse position of the probe was less than 1 mm.

3. Basic flow patterns

The inflow conditions were quiescent for all investigated flow conditions. Next to the upstream edge of the weir crest, the flow accelerated above the crest and became supercritical on the downstream steep slope. The downstream water level did not affect the upstream flows. Next to the upstream end of the crest, the flow was rapidly varied and characterised by a rapid change in pressure and velocity distributions (see below). For all investigated flow conditions, the flow depth was recorded in the middle of the weir crest, and results are presented in Fig. 2, where d_{crest} was measured at $x/L_{crest} = 0.46$, and x is the streamwise distance from the upstream end of the crest (Fig. 1). Note that the critical flow depth is $d_c = 2/3 * H_1$. The results (Fig. 2) indicated that, at mid crest ($x/L_{crest} = 0.46$), the flow was slightly supercritical for low heads above the crest and that it became subcritical at the larger flow rates. The trend is consistent with earlier studies (e.g. [21,8]), and the data exhibited further little difference between all four geometries.

Visual observations showed that the flow above the broad-crest was neither smooth nor stationary for all investigated flow conditions listed in Table 1. Corner eddies were observed next to the sidewalls immediately upstream of the vertical upstream wall (Fig. 1). These spiral vortices with vertical axis looked like "tornadoes". Similar spiral vortices were illustrated by Rouse [16, pp. 75 & 271] and Baud and Hager [1]. They are believed to result from secondary flow motion at the base of the weir, with the strongest effects next to the sidewalls. At relatively regular intervals, one or both eddies grew up and was ejected. The ejected fluid was advected above the weir and spread across the weir. The water level above the weir was strongly affected by the ejection and advection processes. Each ejection was typically associated with a rise in water level above the crest. When one eddy was ejected, its influence spread typically about half the crest width as it reached the downstream end of the broad-crest. If both corner vortices were ejected together, they induced a rise in water level on both the right and left sides of the overflow, while a "trough" was observed on the crest centreline.

Dimensional analysis implies that the occurrence and strength of the vortices must be functions of the relative weir height $H_1/\Delta z$, relative width $B/\Delta z$ and flow Reynolds number $Q/(B * \nu)$; hence the size of the experiment. Herein "tornado" eddies were not seen in the small broad-crested weir operating with $0.232 \leq H_1/\Delta z$, $B/\Delta z = 3.9$ and $Q/(B * \nu) \leq$ 2E+4, but they were always observed in the large facility for $H_1/\Delta z \leq 0.39$, $B/\Delta z = 1$ and 3E+4 $\leq Q/(B * \nu) \leq$ 3E+5. In the present study, the effect of vortex ejection on the overflow appeared to be the strongest for $0.15 \leq H_1/\Delta z \leq 0.39$. The corner vortex ejection rate was recorded in Geometry 4. The average dimensionless frequency was best correlated as

$$\frac{F_{ej} * d_c}{V_c} = 0.0154 * \exp\left(4.12 * \frac{H_1}{\Delta z}\right) \quad 0.22 \leq H_1/\Delta z \leq 0.4 \tag{2}$$

where F_{ej} is the vortex ("tornado") ejection frequency and $V_c = Q/(B * d_c)$.

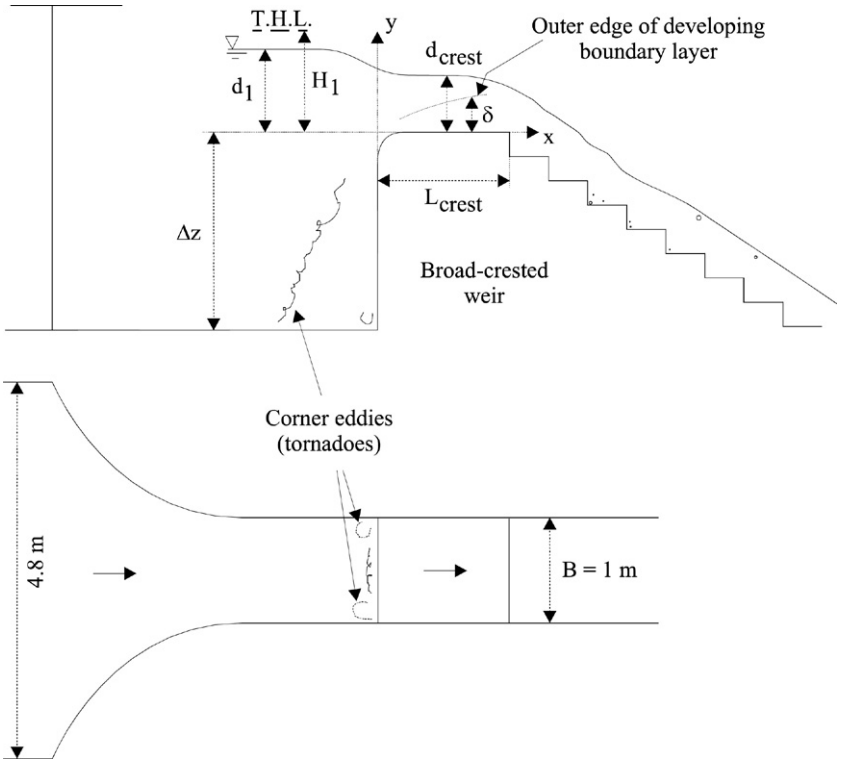

(a) Geometries 1, 2 and 4.

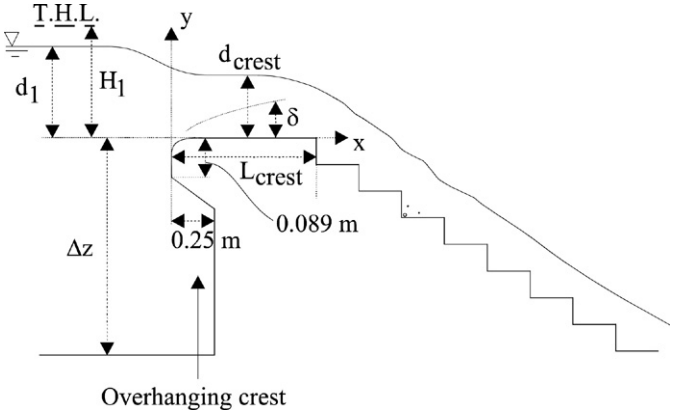

(b) Geometry 3.

Fig. 1. Definition sketches.

4. Velocity and pressure distributions

Velocity and pressure profiles were measured on the upstream half of the crest for a range of flow conditions in Geometries 3 and 4. Both configurations had an identical weir crest length and height, but Geometry 3 had a 0.25 m corbel (Fig. 1). The experimental data showed consistently significant redistributions of pressure and velocity distributions at the upstream end of the broad crest (Fig. 3). For $x/L_{crest} < 0.2$, the pressure gradient was typically less hydrostatic, and the velocity profile had a shape close to that predicted by ideal-fluid flow theory and flow net considerations. Typical experimental data are presented in Fig. 3, and details of the flow conditions are summarised in the figure caption. Fig. 3(a) shows dimensionless velocity distributions along the crest for two geometries and the same water depth above the crest. Fig. 3(b) illustrates the corresponding dimensionless pressure distributions; the solid line (slope 1:1) is the hydrostatic pressure distribution. Fig. 4 presents a simplified flow net analysis (four stream tubes) for the same flow conditions as in Fig. 3. The sketch is undistorted, and equipotentials are not shown for clarity.

The rapid flow redistribution at the upstream end of the weir crest was associated with the development of a turbulent boundary layer. At the upstream end of the crest, the flow is essentially irrotational, but friction, and the no-slip condition, at the boundary affect the velocity on the crest invert. The boundary layer development was calculated from measured

Table 1
Experimental investigations of horizontal broad-crested weirs

Experiment	L_{crest}	Δz	B	Q	H_1	$\frac{H_1}{L_{crest}}$	Remarks
	m	m	m	m^3/s	m		
(1)	(2)	(3)	(4)	(5)	(6)	(7)	(8)
Sharp-edged weir							
[2]	0.40	0.75	2.0	–	0.064 to 0.402	0.159 to 1.0	Sér. 113.
	0.80	0.75	2.0	–	0.062 to 0.42	0.0779 to 0.527	Sér. 114.
	1.99	0.75	2.0	–	0.06 to 0.447	0.03 to 0.225	Sér. 115.
[21]	3.05	0.533	0.6096	–	0.1524 to 0.457	0.05 to 0.2	
[20]	1.80	0.30	0.50	0.0073 to 0.041	0.042 to 0.132	0.023 to 0.073	
[15]	0.10 to 3.0	0.3	0.610	up to 0.14	0.03 to 0.25	0.017 to 1.9	
[13]	0.15	0.152	0.610	–	0.051 & 0.76	0.336 & 0.5	
	0.381	0.152	0.610	–	0.038	0.10	
	0.762	0.152	0.610	–	0.033 & 0.048	0.043 & 0.063	
Rounded-edged weir							
[2]	0.90	0.75	2.0	–	0.054 to 0.402	0.06 to 0.446	$R = 0.10$ m. Sér. 116.
	2.09	0.75	2.0	–	0.048 to 0.407	0.023 to 0.195	$R = 0.10$ m. Sér. 117.
[21]	3.05	0.533	0.6096		0.1524 to 0.457	0.05 to 0.2	$R = 0.051$ to 0.203 m.
[10]	0.42	0.0646	0.25	0.001–0.07	0.015 to 0.0675	0.036 to 0.161	
Present study							
Geometry 1	0.60	0.90	1.0	0.046 to 0.182	0.09 to 0.225	0.15 to 0.375	$R = 0.057$ m. Vertical upstream wall.
Geometry 2	0.88	0.90	1.0	0.05 to 0.26	0.096 to 0.29	0.10 to 0.32	$R = 0.057$ m. Vertical upstream wall.
Geometry 3	0.617	0.99	1.0	0.0064 to 0.17	0.023 to 0.21	0.037 to 0.337	$R = 0.057$ m. 0.25 m overhanging crest.
Geometry 4	0.617	0.99	1.0	0.0064 to 0.21	0.023 to 0.24	0.037 to 0.39	$R = 0.057$ m. Vertical upstream wall.
Small weir	0.42	0.0646	0.25	0.001 to 0.005	0.015 to 0.075	0.036 to 0.18	Vertical upstream wall.

Notes: H_1 upstream head above crest elevation; Q: water flow rate; R: radius of curvature; (–): not available.

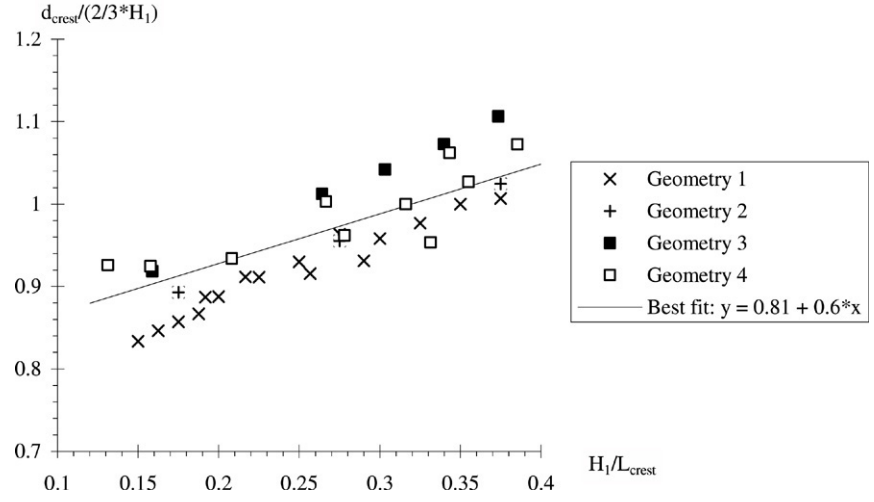

Fig. 2. Dimensionless water depth on the weir crest (measured at $x/L_{crest} = 0.46$).

velocity profiles. Results are presented in Fig. 5. The boundary layer thickness data were best correlated by

$$\frac{\delta}{x} = 0.549 * \left(\frac{x}{k_s}\right)^{-0.436} \quad (3)$$

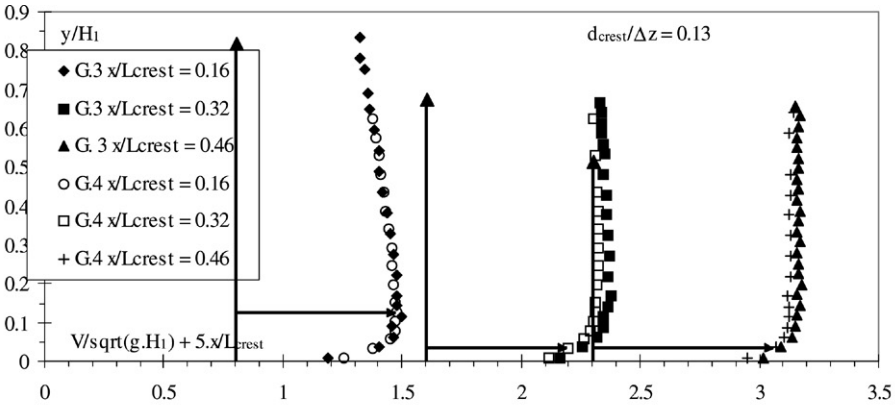

(A) Dimensionless velocity distributions $V/\sqrt{g*H_1}$ as functions of y/H_1 - The horizontal axis is $V/\sqrt{g*H_1} + 5*x/L_{crest}$.

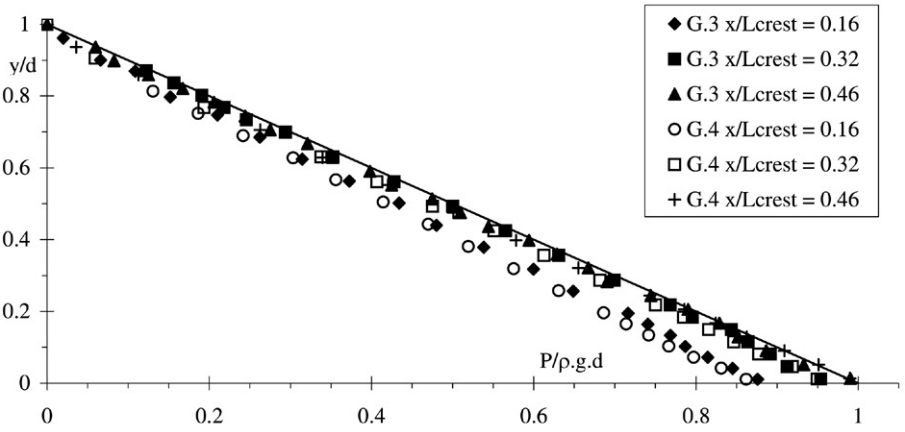

(B) Dimensionless pressure distributions $P/(\rho*g*d)$ as function of y/d - Comparison with the hydrostatic pressure distribution.

Geometry	H_1 (m)	d (m) x/L_{crest}=0.16	d (m) x/L_{crest}=0.32	d_{crest} (m) x/L_{crest}=0.46	Q (m^3/s)	Remark
Geometry 3	0.1871	0.163	0.1455	0.130	0.143	Overhanging crest
Geometry 4	0.2045	0.162	0.1455	0.130	0.145	Vertical upstream wall

Fig. 3. Dimensionless velocity and pressure distributions on the weir crest ($d_{crest}/\Delta z = 0.13$).

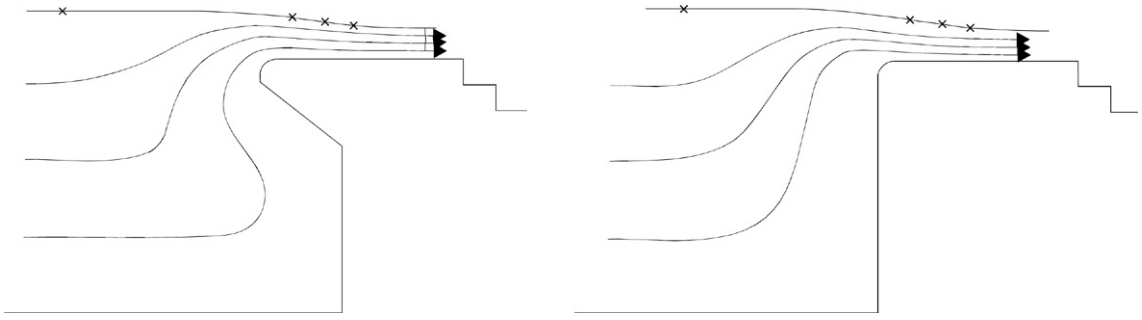

Fig. 4. Simplified flow net analysis for the same flow conditions as in Fig. 3.

where δ is the boundary layer thickness defined in terms of 99% of the free-stream velocity and k_s is the equivalent sand roughness height (herein $k_s = 0.5$ mm). The boundary layer growth was about $\delta \sim x^{0.57}$, compared to a smooth turbulent

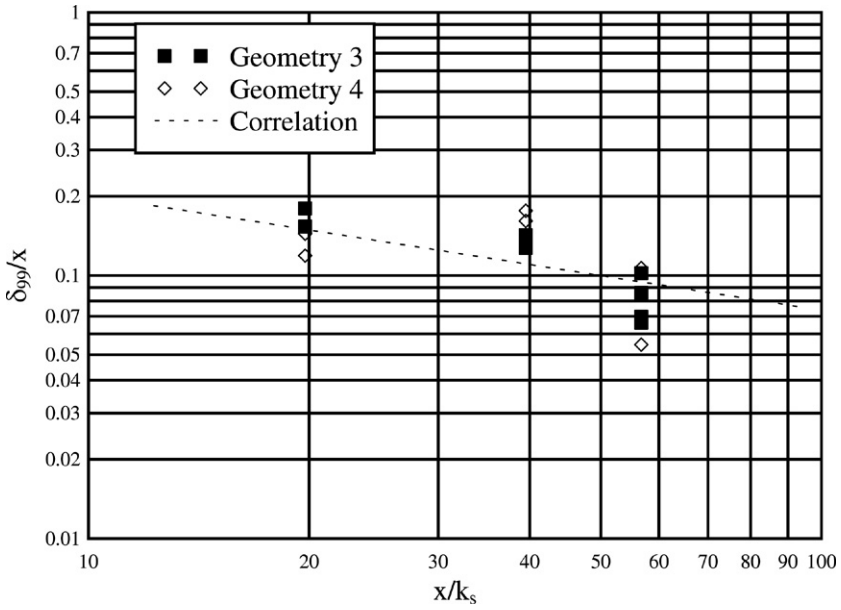

Fig. 5. Dimensionless boundary layer thickness for Geometries 3 and 4 ($x/L_{crest} \leq 0.5$). Comparison with Eq. (3).

layer growth of $\delta \sim x^{0.8}$. Note that the virtual origin of the boundary layer was a short distance upstream of the upstream end of the crest. The data of Guernsey (cited in [8]) indicated the same trend.

The data highlighted some differences in terms of velocity and pressure distributions between Geometries 3 and 4 (Fig. 3). These differences were caused by the overhanging crest (or corbel) design and they were observed on the entire flow field (pressure and velocity distributions). They are believed to be caused by different inflow streamline patterns (Fig. 4).

5. Discussion: Discharge coefficient estimate

The discharge per unit width was calculated from the integration of the measured velocity profiles:

$$\frac{Q}{B} = \int_{y=0}^{d} V * \mathrm{d}y \tag{4}$$

where y is the vertical distance measured from the crest invert, d is the local flow depth and V is the velocity. The data are summarised in Fig. 6 in terms of the dimensionless discharge coefficient C_D (Eq. (1)) and they are compared with previous studies obtained with upstream rounded-edges and square-edges. Fig. 6 illustrates the lower discharge capacity of square-edged weirs, and [13] demonstrated the adverse role of the upstream separation bubble on the flow streamlines.

Present results showed contrasting trends between Geometry 3 and Geometry 4. The latter has a vertical upstream wall while the former had an overhanging crest (Fig. 1). In Geometry 3, the data yielded an increasing discharge coefficient with increasing head above the crest as observed by Rouse [17] and Harrison [8]. With Geometry 4, present results suggested a slight decrease in discharge coefficient with increasing head above the crest, although the data are scattered. Visual observations showed significant flow disturbances induced by the corner eddies. It is hypothesised that the trend for Geometry 4 was the result of these overflow disturbances that appeared the strongest for the largest investigated flow rates.

Overall, the dimensionless discharge coefficient data was best correlated by

$$C_D = 1.242 * \left(\frac{H_1}{L_{crestf}}\right)^{0.1533} \quad \text{Geometry 3} \tag{5}$$

$$C_D = 1.013 - 0.228 * \frac{H_1}{L_{crest}} \quad \text{Geometry 4} \tag{6}$$

for $0.12 \leq H_1/L_{crest} \leq 0.38$.

Note that the overhanging crest design, also called offset or corbel, is used with ogee crests (e.g. [11,6]). Usually, the discharge coefficient differs from classical ogee crest results if the offset thickness is less than one third of the design head above the crest [6,19].

6. Conclusion

Basic experiments were conducted in a near-full-scale broad-crested weir. The study showed rapid redistributions of both velocity and pressure fields at the upstream end of the weir crest. These were rarely studied in a large-size facility under controlled flow conditions. Within the investigated flow conditions, large vortical structures were observed immediately upstream of the weir crest, and these induced non-stationary flow conditions affecting the overflow. Pressure and velocity distributions measurements were conducted systematically for two configurations. The comparative results showed some differences between the two geometries, all other parameters being equal, induced by a corbel design. Correlations were derived for the dimensionless discharge coefficient in both cases.

Comparative experiments in small-size and large-size flumes suggested that complicated weir overflow patterns might be

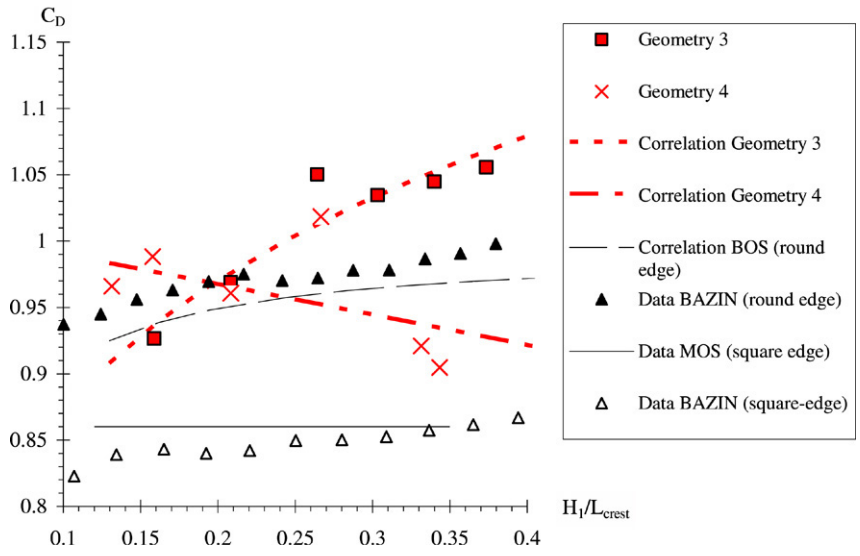

Fig. 6. Dimensionless discharge coefficients for Geometries 3 and 4. Comparison with Eqs. (5) and (6), and previous studies with square-edge [2,13] and rounded edge [2,4].

observed in prototype structures. Further studies would be required to clarify the flow conditions and weir geometry that might be adversely affected by large-scale vortices.

Acknowledgments

The writers acknowledge the technical assistance of Graham Illidge (The University of Queensland). The first writer is grateful for the financial support of the National Council for Science and Technology of Mexico (CONACYT).

References

[1] Baud O, Hager WH. Tornade vortices in settling tanks. J Environ Eng ASCE 2000;126(2):189–91.
[2] Bazin H. Expériences Nouvelles sur l'Ecoulement par Déversoir ('Recent experiments on the flow of water over weirs'). In: Mémoires et Documents, Annales des Ponts et Chaussées, Sér. 7, vol. 12. 2nd Sem. 1896. p. 645–731. Plates [in French].
[3] Belanger JB. Notes sur le Cours d'Hydraulique ('Notes on the hydraulics subject'). In: Mém. Ecole Nat. Ponts et Chaussées. 1849 [in French].
[4] Bos MG. Discharge measurement structures. Publication No. 161, Delft Hydraulic Laboratory, Delft, The Netherlands. 1976 (also Publication No. 20, ILRI, Wageningen, The Netherlands).
[5] Chanson H. The hydraulics of open channel flows: An introduction. 2nd edition. Oxford, UK: Butterworth-Heinemann; 2004. p. 630.
[6] Davis CV, Sorensen KE. Handbook of applied hydraulics. 3rd ed. New York, USA: McGraw-Hill; 1969.
[7] Hall GW. Analytical determination of the discharge characteristics of broad-crested weirs using boundary layer theory. Proc Inst Civ Eng 1962; 22:177–90. paper No. 6607.
[8] Harrison AJM. The streamlined broad-crested weir. Proc Inst Civil Eng 1967;38:657–678; Discussion 1969;42:575–99.
[9] Henderson FM. Open channel flow. New York, USA: MacMillan Company; 1966.
[10] Isaacs LT. Effects of laminar boundary layer on a model broad-crested weir. Research Report No. CE28. Brisbane (Australia): Dept. of Civil Eng., Univ. of Queensland; 1981. 20 pages.
[11] Kirkpatrick HKW. Discharge coefficients for spillways at TVA dams. Trans ASCE 1957;122:190–210.
[12] Montes JS. The streamlined broad-crested weir. Discussion. Proc Inst Civil Eng 1969;42:576–8.
[13] Mos WD. Flow separation at the upstream edge of a square-edged broad-crested weir. J Fluid Mech 1972;52(Part 2):307–20, 1 plate.
[14] Ramamurthy AS, Tim US, Rao MVJ. Characteristics of square-edged and round-nosed broad-crested weirs. J Irrig Drainage Engrg ASCE 1988; 114(2):61–73.
[15] Rao NSGovinda, Muralidhar D. Discharge characteristics of weirs of finite crest width. J La Houille Blanche 1963;18(5):537–45.
[16] Rouse H. Fluid mechanics for hydraulic engineers. New York, USA: McGraw-Hill Publ.; 1938 (also Dover Publ., New York, USA, 1961, 422 pages).
[17] Rouse H. Engineering hydraulics. In: Proc. 4th Hyd. Conf., IIWR. New York, USA: John Wiley & Sons; 1949.
[18] Serre F. Contribution à l'Etude des Ecoulements Permanents et Variables dans les Canaux [Contribution to the study of permanent and non-permanent flows in channels]. J La Houille Blanche 1953;830–72 [in French].
[19] Thomas HH. The engineering of large dams. London, UK: John Wiley & Sons; 1976 (2 volumes).
[20] Tison LJ. Le Déversoir Epais [Broad-crested weir]. J La Houille Blanche 1950;426–39 [in French].
[21] Woodburn JG. Tests of broad-crested weirs. Trans ASCE 1932;96: 387–416; Discussion 1932;96:417–53.